Supporting Information

Johansson *et al.* 10.1073/pnas.0805827105

SI Materials and Methods

Octahistidine Tagging of the Chromosomal Gene and Purification of Fatty Acid Synthase from *S. cerevisiae*. A PCR-generated fragment coding for a His_8 tag was integrated into the *FAS1* gene by homologous recombination. This strategy resulted in a haploid yeast strain with a C-terminally modified β- and unmodified α-chain. The introduction of the His tag did not interfere with cell growth and allowed fast and efficient purification of the FAS complex. Ni-NTA affinity chromatography was used as a first purification step; fractions enriched with FAS were further purified by ultra-centrifugation. The purification progress was routinely monitored by assaying the FAS enzymatic activity. The purity of the protein was >95%, as judged from Coomassie stained SDS/PAGE gels. In a typical protein preparation, 5–10 mg of protein was obtained from 2 liters of yeast culture.

Enzyme Activity. In the biosynthesis of fatty acids by the *S. cerevisiae* FAS, acetyl-CoA is used as a starting unit and successively condensed with malonyl-CoA. The keto functionality introduced by the condensation reaction is reduced in two steps by the consumption of two equivalents of NADPH. The specific enzyme activity was therefore monitored by the change in absorption at 334 nm; the specific activity of the purified enzyme was 800 to 1,200 milliunits/mg protein (Fig. S2) (1).

Cryo-EM and Image Processing. Samples of the protein were applied to glow-discharged Quantifoil grids (Quantifoil Micro Tools GmbH) and vitrified by plunging into liquid ethane by using a Vitrobot plunge-freezing device (FEI). Data were collected on a Tecnai G2 Polara microscope operating at 300 kV. Images were taken at a magnification of ×39,000 on Kodak SO-163 film and scanned on a Photoscan scanner (Intergraph) at a step size of 7 μm. Adjacent pixels were averaged to yield a step size of 3.59 Å on the specimen. Particles were selected by using the semiautomatic mode of the BOXER module from EMAN (2) and 3D reconstruction by angular reconstitution from ≈20,000 particles was done by using IMAGIC V (3). The resolution of the model was determined by Fourier Shell Correlation to be 16 Å by the 3 σ criterion.

Crystallization. Crystallization trials were set up with purified FAS at concentrations of 6–12 mg/ml in buffer A [100 mM sodium phosphate (pH 6.5)] by using the vapor diffusion hanging-drop technique at 4°C. Initial trials were performed by using commercially available screens (Hampton Research). Diffracting crystals grew in 0.1 M Hepes (pH 7), 1 M ammonium sulfate, and PEG of various chain lengths [4,000 (14%), 3,350 (15%), 3,000 (15%), 2,000 (15%), and 1,500 (17%)]. Crystals were optimized by using additives such as 0.1 M L-proline, 5–20% palmitic acid in chloroform or ethanol, 0.1 M hexamidine Co(III) chloride, or 20% wt/vol benzamidine·HCl. Crystals grew in a bipyramidal shape, except when by using palmitic acid as an additive which led to spike shaped crystals.

Data Collection and Processing. The elongated FAS crystals tended to orient in cryoloops with the long axis parallel to the x-ray beam, resulting in diffraction spot overlap. By using bent cryoloops and a kappa-arc at the Swiss Light Source (SLS) or the minikappa goniostat at the European Synchrotron Radiation Facility (ESRF), samples were mounted with the long crystallographic axis as far as possible from the incident beam.

X-ray data were collected at beamlines X10SA (SLS) and ID14 EH1–4, ID23 EH1–2, and ID29 (ESRF). The effective resolution of native and heavy atom soaked crystals was in most cases limited by radiation damage. Complete native, Ta_6Br_{12}, and W_{18} data were collected to 4, 6, and 7 Å, respectively, and processed by using MOSFLM (4), XDS (5), D*TREK (6), and SCALA (7) (Table 1). All crystals were found to belong to space group $P4_12_12/P4_32_12$ with unit cell parameters of ≈231 × 231 × 754 Å. Assuming the asymmetric unit to contain one FAS particle gave a V_M value of 1.9 Å^3 Da^{-1}, corresponding to a solvent content of 37% (8). However, a self-rotation function of the data indicated the principal 3-fold symmetry of the complex to be perpendicular to a crystallographic 2-fold axis, suggesting that the asymmetric unit might only contain half a FAS particle. This was later confirmed by using the initial heavy atom positions and GETAX (9), yielding a solvent content of 68%.

Four sites could be located in the Ta_6Br_{12} dataset by direct methods by using SHELX (10). Initial phase estimates using spherically averaged Ta clusters were calculated by SHARP (11). By careful stepwise density modification with the use of SOLOMON (12) and DM (13), phases were considerably improved. Subsequent calculation of anomalous and isomorphous log-likelihood gradient and difference Fourier maps facilitated the location of a number of weaker sites in the Ta_6Br_{12} and the W_{18} datasets. After phase-restrained refinement of the new heavy atom cluster substructure in SHARP, the updated MIRAS phases were subjected to statistical density modification in PIRATE (K. Cowtan, unpublished) by using the PDB reference structures 1T5E, 1AV1, and 1XA6, selected on the basis of initial E correlation. The new density modified maps in combination with the EM data enabled the identification of most of the separate domains of the FAS particle, allowing the original averaging mask to be updated. A final run of solvent flattening, histogram matching, and averaging in DM further extended the phases to ≈ 4.5 Å (Fig. S4).

Manual rebuilding of the ≈5,000 CA polypeptide backbone built by the automatic chain-tracing program Buccaneer (Kevin Cowtan, unpublished) had just been initiated when the *T. lanuginosus* and *S. cerevisiae* fatty acid synthase structures were published by Ban and coworkers (14, 15). The 3.1 Å model of the *S. cerevisiae* core-FAS complex (PDB ID code 2UV8) was placed onto the CA-trace, by using the LSQ tools of O (16). Initial phase-restrained rigid body refinement was performed in Refmac5 (17) to a resolution of 6 Å. The phase-restraints were kept during NCS-restrained domain-wise rigid body cycles in phenix.refine (18) to a resolution of 4 Å. Resulting $F_o - F_c$ and $2F_o - F_c$ maps were used for very minor model rebuilding in O and Coot (19). Final NCS-restrained domain-wise rigid-body refinement with grouped B-factors gave an R/R_{free} 27%/27% after bulk solvent correction and anisotropic scaling (20), reflecting the placement of the rigid high resolution structure in the low resolution data. An averaged $F_o - F_c$ map showed clear density for 8 of the 12 carbons of the CER backbone (Fig. 2 *A* and *B*). After adjusting the chi angles of the KS active-site side chains C1305, F1646 and M1251, as seen in omit maps, the C9–C12-truncated cerulenin molecule was subjected to NCS-restrained refinement together with a sphere of residues surrounding the binding pocket, keeping the rest of the structure fixed. CER C1–C4 exhibited good $2F_o - F_c$ density, whereas density for C5–C8 was much weaker. The refined position of both segments could however be verified by calculating an averaged difference Fourier map between the CER dataset and the deposited, cerulenin-free, structure factors from Steitz and coworkers

(PDB ID code 2PFF) (21). Final refinement statistics are given in Table S1. The coordinates and structure factors have been deposited at the PDB with access code 2VKZ.

Structural Differences of *S. cerevisiae* FAS Models. The two published *S. cerevisiae* FAS models from Ban and coworkers (14, 15) and Steitz and coworkers (21) exhibit surprisingly few differences given the relatively low resolution of both structures. However, one main-chain tracing difference between N427 and T536 of the α-chain (Ban numbering) results in a change of topology of a 20-kDa expansion segment that packs onto the KR-domain. An averaged B-factor sharpened (22) omit map calculated from our 4-Å data indicated that the Ban chain-tracing and topology is correct.

In contrast to the two Ban models, the Steitz 4-Å structure also included the exterior PPT domain, responsible for the addition of the carrier 4′-phosphopantetheine to the FAS ACP (23). Weak density for the PPT domain attached to the C terminus of the α-chain could be seen in our crystallographic $F_o - F_c$ maps but not in the cryo-EM map. Conversely, the exterior four-helix KR bundle, N537–E581, seen in the Ban *T. lanuginosus* FAS complex (15) but not in any of the two *S. cerevisiae* structures, was clearly seen in the cryo-EM map, but not in our crystallographic electron density maps (Fig. S3).

Five regions in the α-chain and three regions in the β-chain showed sequence register differences between the Ban and the Steitz structures. In the case of α-chain Q989–D1014, N1064–T1197, and G1424–K1446, our maps clearly support the Ban model. The sequence threading of α-chain Q1620–V1636 and K1726–I1738 (Ban numbering), however, could not be unambiguously determined. In the segment N1716–N1737 of the β-chain, the sequence of the Ban structure was substantiated, whereas the sequence decoration of R1861–P1957 and S5–Q79 could not be verified with our data.

1. Kawaguchi A, Tomoda H, Nozoe S, Omura S, Okuda S (1982) Mechanism of action of cerulenin on fatty acid synthetase. Effect of cerulenin on iodoacetamide-induced malonyl-CoA decarboxylase activity. *J Biochem* 92:7–12.
2. Ludtke SJ, Baldwin PR, Chiu W (1999) EMAN: Semiautomated software for high-resolution single-particle reconstructions. *J Struct Biol* 128:82–97.
3. van Heel M, Harauz G, Orlova EV, Schmidt R, Schatz M (1996) A new generation of the IMAGIC image processing system. *J Struct Biol* 116:17–24.
4. Leslie AGW (1992) Recent changes to the MOSFLM package for processing film and image data. in *CCP4 and ESFEACMB Newsletter on Protein Crystallography*, No. 26 (Daresbury Laboratory, Warrington, UK).
5. Kabsch W (1993) Automatic processing of rotation diffraction data from crystals of initially unknown symmetry and cell constants. *J Appl Crystallogr* 26:795–800.
6. Pflugrath JW (1999) The finer things in X-ray diffraction data collection. *Acta Crystallogr D* 55:1718–1725.
7. Evans PR (1993) in *Proceedings of the CCP4 Study Weekend: Data Collection and Processing*, eds Sawyer L, Isaacs N, Bailey S (Daresbury Laboratory, Warrington, UK), pp 114–122.
8. Matthews BW (1968) Solvent content of protein crystals. *J Mol Biol* 33:491–497.
9. Vonrhein C, Schulz GE (1999) Locating proper non-crystallographic symmetry in low-resolution electron-density maps with the program GETAX. *Acta Crystallogr D* 55:225–229.
10. Schneider TR, Sheldrick GM (2002) Substructure solution with SHELXD. *Acta Crystallogr D* 58:1772–1779.
11. de la Fortelle E, Bricogne G (1997) Maximum-likelihood heavy-atom parameter refinement for multiple isomorphous replacement and multiwavelength anomalous diffraction methods. *Methods Enzymol* 276:472–494.
12. Abrahams JP, Leslie AGW (1996) Methods used in the structure determination of bovine mitochondrial F1 ATPase. *Acta Crystallogr D* 52:30–42.
13. Cowtan K, Main P (1998) Miscellaneous algorithms for density modification. *Acta Crystallogr D* 54:487–493.
14. Jenni S, *et al.* (2007) Structure of fungal fatty acid synthase and implications for iterative substrate shuttling. *Science* 316:254–261.
15. Leibundgut M, Jenni S, Frick C, Ban N (2007) Structural basis for substrate delivery by acyl carrier protein in the yeast fatty acid synthase. *Science* 316:288–290.
16. Jones TA, Zou JY, Cowan SW, Kjeldgaard M (1991) Improved methods for building protein models in electron density maps and the location of errors in these models. *Acta Crystallogr A* 47:110–119.
17. Murshudov GN, Vagin AA, Dodson EJ (1997) Refinement of macromolecular structures by the maximum-likelihood method. *Acta Crystallogr D* 53:240–255.
18. Afonine PV, Grosse-Kunstlev RW, Adams PD (2005) The Phenix refinement framework. *CCP4 Newsletter*, Contribution 8.
19. Emsley P, Cowtan K (2004) Coot: Model-building tools for molecular graphics. *Acta Crystallogr D* 60:2126–2132.
20. Afonine PV, Grosse-Kunstleve RW, Adams PD (2005) A robust bulk-solvent correction and anisotropic scaling procedure. *Acta Crystallogr D* 61:850–855.
21. Lomakin IB, Xiong Y, Steitz TA (2007) The crystal structure of yeast fatty acid synthase, a cellular machine with eight active sites working together. *Cell* 129:319–332.
22. Bass RB, Strop P, Barclay M, Rees DC (2002) Crystal structure of *Escherichia coli* MscS, a voltage-modulated and mechanosensitive channel. *Science* 298:1582–1587.
23. Fichtlscherer F, Wellein C, Mittag M, Schweizer E (2000) A novel function of yeast fatty acid synthase. Subunit alpha is capable of self-pantetheinylation. *Eur J Biochem* 267:2666–2671.

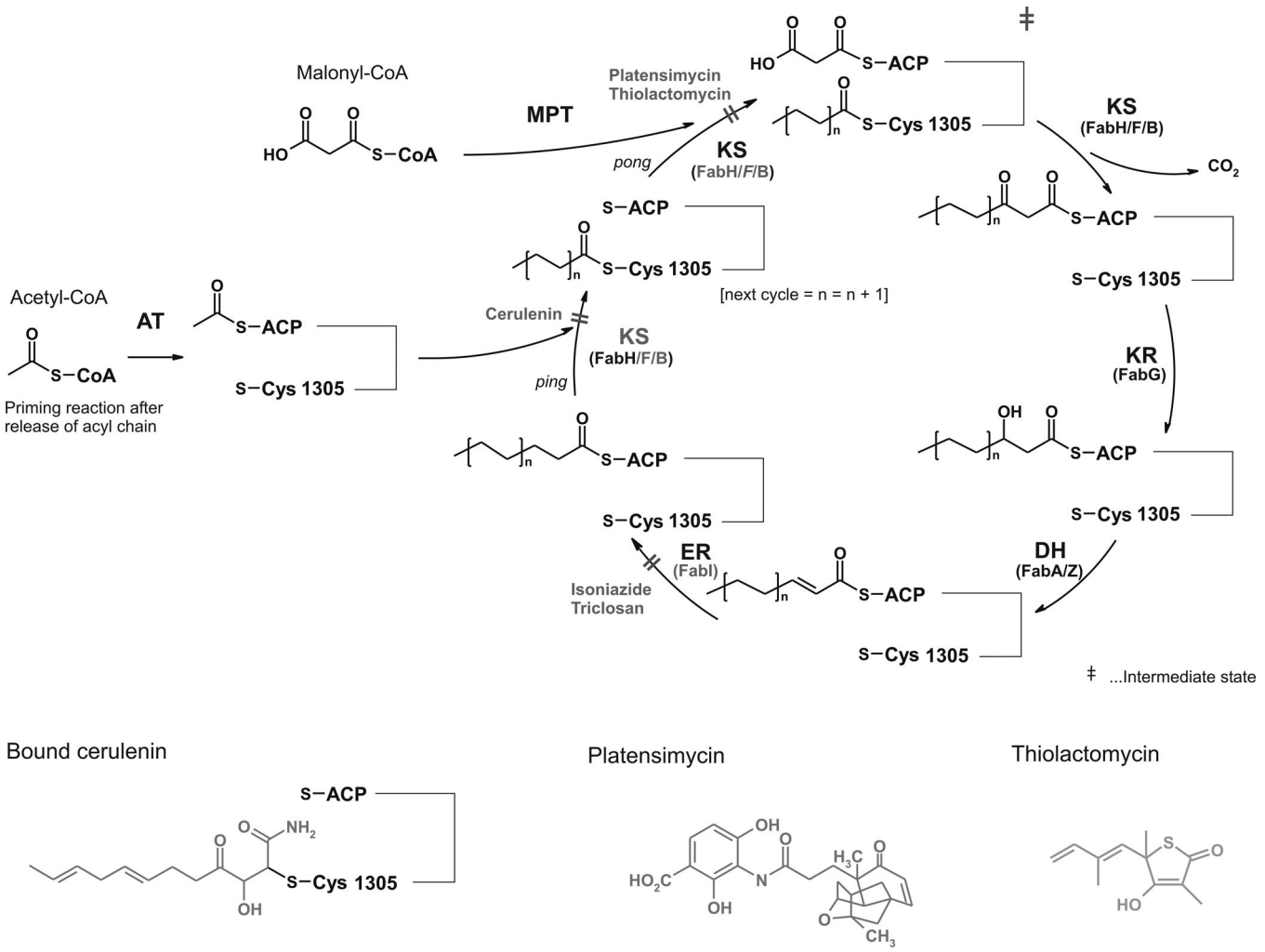

Fig. S1. The fatty acid synthase cycle. Cerulenin inhibits the ping step of the ketoacyl synthase mechanism, whereas thiolactomycin and platensimycin inhibits the pong step. The enoyl reductase (ER) inhibitors triclosan and isoniazid are included for reference. Bacterial enzyme names are indicated between brackets.

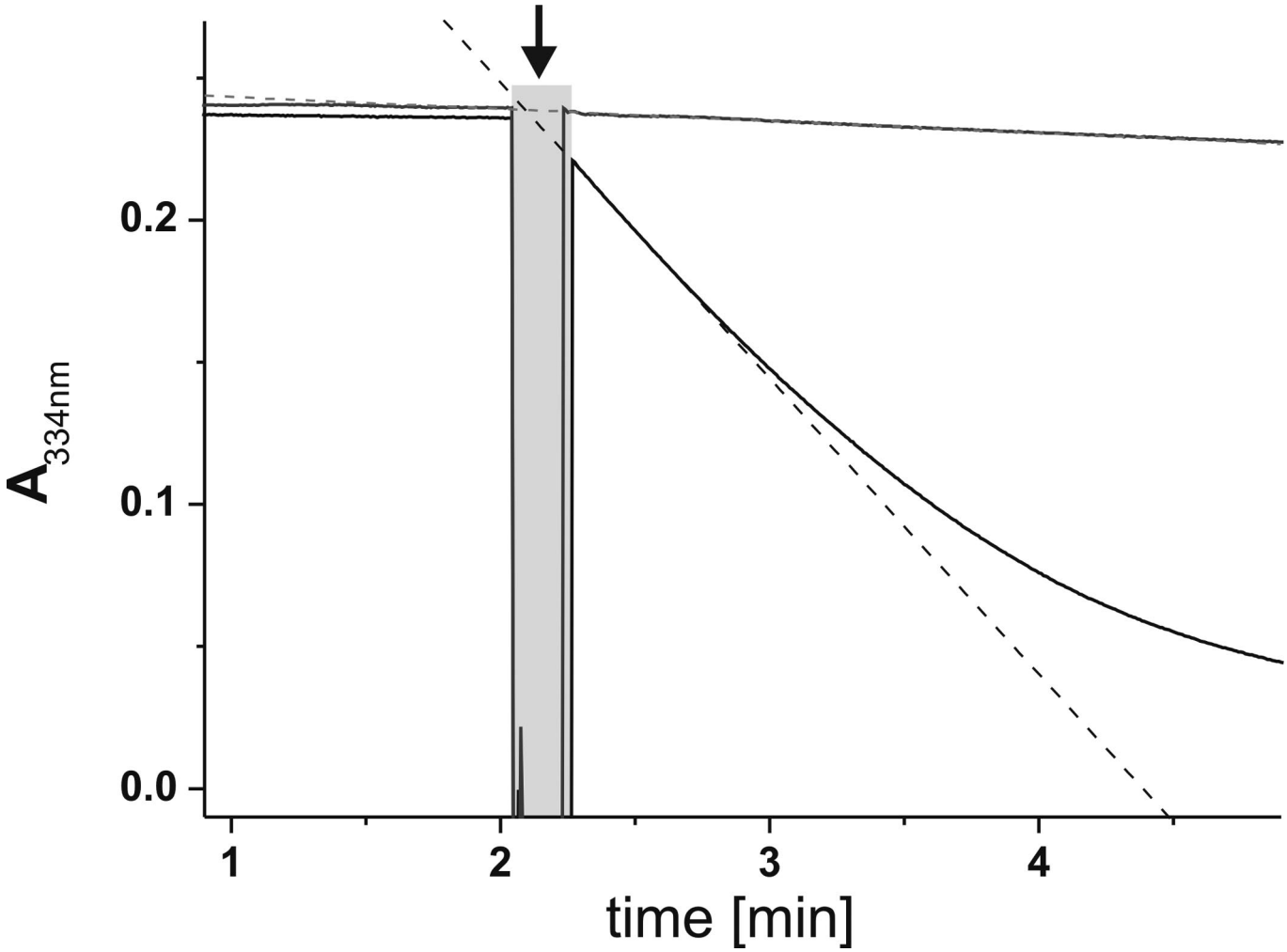

Fig. S2. Inhibition of FAS by cerulenin. Readout functions of activity assays preformed on noninhibited (black) and inhibited (gray) FAS. The gray rectangle marks displacement of cuvette for start of fatty acid synthesis reaction by addition of malonyl-CoA (arrow). The dashed lines are fit functions for calculating activity. After inhibition the remaining activity is 2.5% (3,977 vs. 100 milliunits/ml).

Fig. S3. Cryo-EM map superposition. A slice of the yeast FAS model and the EM density at the equator shows the three missing four-helix KR bundles, located at the perimeter of the α_6-wheel.

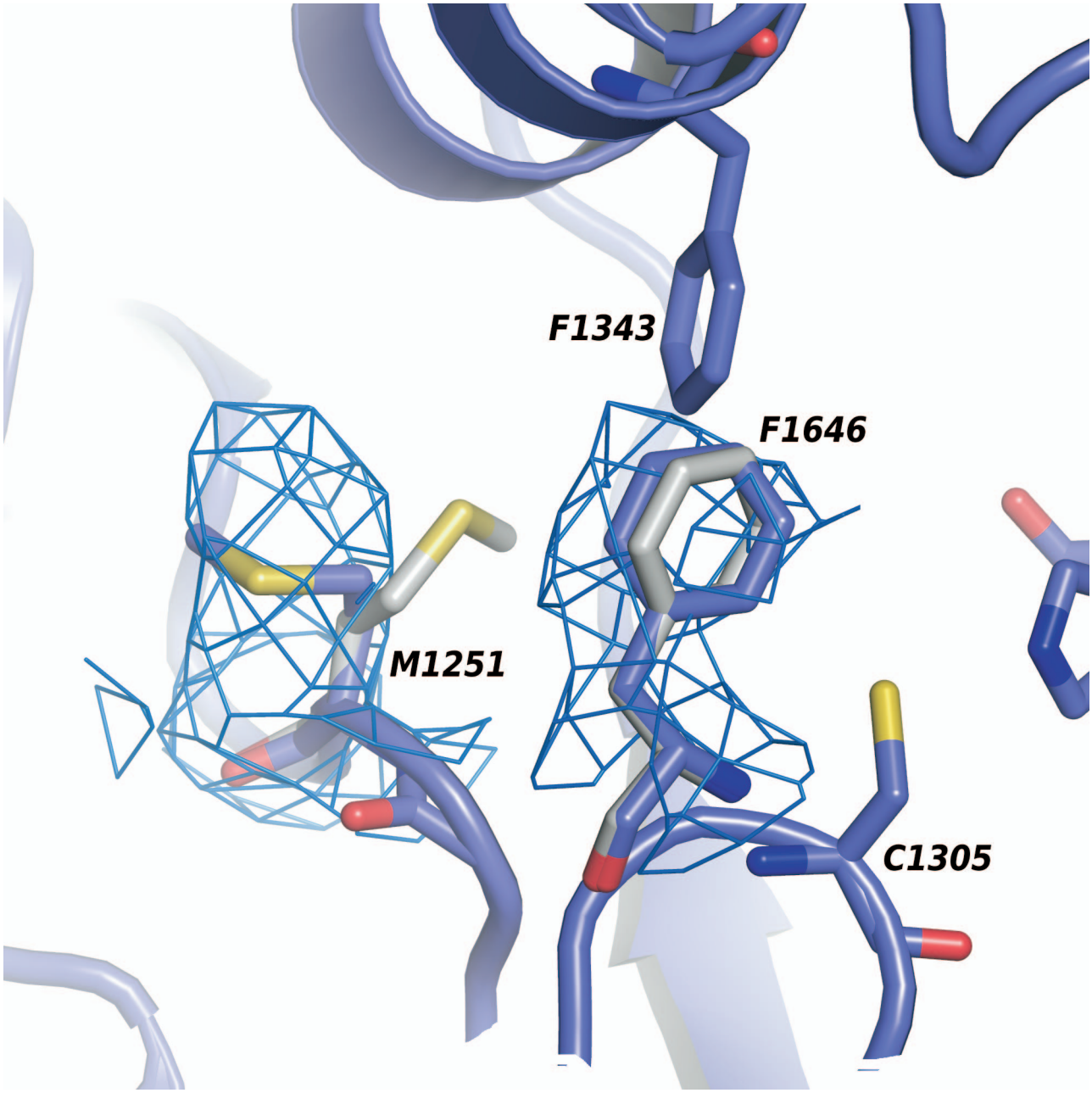

Fig. S4. Difference electron density for side chains M1251 and F1646. An averaged B-factor sharpened $2F_o - F_c$ map with M1251 and F1646 omitted shows the flipped conformation of the FAS–CER (blue) compared to the native FAS structure (gray). The map was contoured at 1.5 σ within a radius of 2.5 Å.

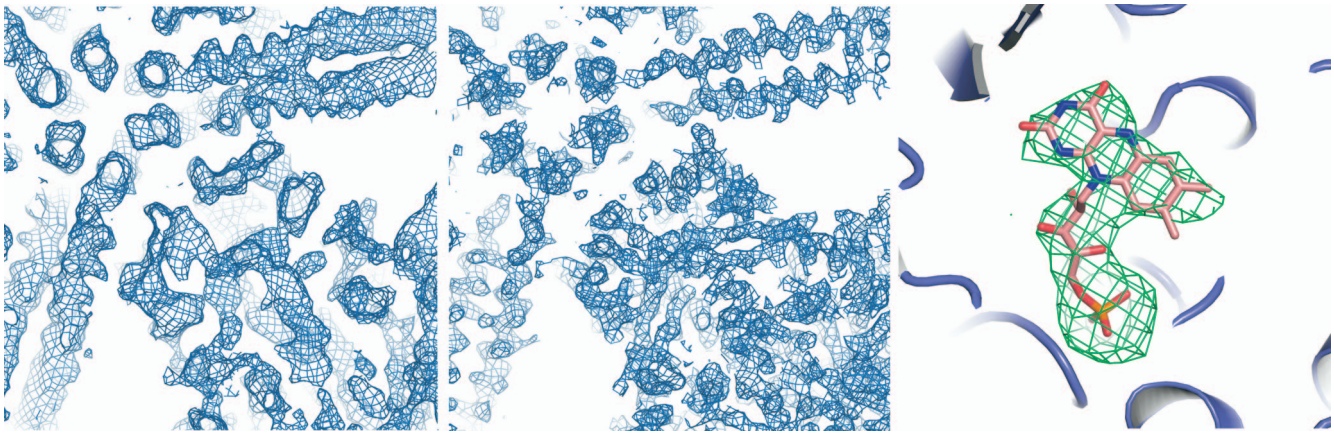

Fig. S5. Examples of experimental and refined phases. (*Left*) Initial B-factor sharpened averaged map from DM, contoured at 1.5. (*Center*) Final B-factor sharpened $2F_o - F_c$ map with the helical spokes (L328–Y377) omitted, contoured at 1.5 σ. (*Right*) $F_o - F_c$ omit map of the flavin mononucleotide (FMN) cofactor of the FAS enoyl reductase domain, contoured at 3 σ within a radius of 3Å.

Table S1. Data collection, phasing, and refinement statistics

	Native (CER)	Ta_6Br_{12}	W_{18}
Data collection			
Space group	$P4_32_12$	$P4_32_12$	$P4_32_12$
Cell dimensions *a*, *b*, and *c*, Å	231.9, 231.9, 756.8	232.0, 232.0, 751.1	231.1, 231.1, 751.3
Resolution, Å	25.0–4.0	40.0–6.0	30.0–7.0
R_{merge}	0.24 (>1)	0.21 (>1)	0.36 (>1)
$I/\sigma I$	7.0 (1.4)	15.8 (1.1)	4.24 (1.2)
Completeness, %	98.0 (98.0)	100.0 (100.0)	99.6 (99.7)
Redundancy	3.2 (3.2)	13.9 (12.3)	7.2 (7.3)
Phasing			
Number of sites		14	21
PP, Ano/Iso (acentric)		0.46/0.56	0.84/1.49
R_{Cullis}, Ano/Iso (acentric)		0.97/0.69	0.93/0.66
Refinement			
Resolution, Å	25.0–4.0		
No. of reflections	168,779		
R_{work}/R_{free}	0.27/0.27		
No. of atoms			
Protein	85,830		
Ligand/ion	129		
Average B factors			
Protein, $Å^2$	164.2		
Ligand/ion, $Å^2$	160.4		
rmsd			
Bond lengths, Å	0.010		
Bond angles, °	1.16		

Values in parentheses refer to the highest-resolution shell.